Bunched beam envelope equations including image effects from a cylindrical pipe

Christopher K. Allen*
Techno-Sciences, Inc., 10001 Derekwood Lane, Suite 204, Lanham, Maryland 20706

Martin Reiser†
Institute for Plasma Research, University of Maryland, College Park, Maryland 20742

(Received 30 January 1997)

We derive a set of differential equations for the beam envelopes of an axisymmetric, bunched beam inside a perfectly conducting beam pipe. It is found that the beam dynamics are essentially independent of the form of bunch distribution in the free-space situation, however, in the presence of the beam pipe this is no longer the case. Analytic expressions involving infinite summations of Bessel functions are derived for the image potential and image fields of an ellipsoidally symmetric charge distributions in a beam pipe, in particular, the uniform density distribution. We simulate a simple beam transport system to demonstrate the application of these results. [S1063-651X(97)11806-2]

PACS number(s): 29.27.Bd, 41.85.Ja, 29.27.Eg, 41.75.−i

I. INTRODUCTION

In this paper we derive differential equations describing the dynamics of a bunched beam's rms envelopes. The major contribution here is the inclusion of image effects from a cylindrical beam pipe in the beam dynamics. Also included are analytic expressions for the electrostatic image potential of an ellipsoidal charge distribution in a perfectly conducting cylinder, in particular for a uniform density ellipsoid. These potentials are expressed as infinite summations of Bessel functions, and to our knowledge, have never been published previously. The free-space potentials for these distributions are already known [1,2], thus the full electrostatic potential, including images, may be constructed analytically.

In the bunched beam situation the image effects may substantially alter the beam dynamics. When the bunch length has a comparable dimension to the pipe diameter, images forces may be on the same order as the free-space self-forces. Since many applications use bunch lengths in this range and larger, image effects must be considered. Newton considered this problem over 30 years ago [3]. He provided a very complete mathematical treatment of bunched beams in accelerators. As well as image forces, he included resistive walls and dielectrics in his exposition. However, his final results were computed numerically and he was unable to provide any simple analytic models.

In the late 1970s Neuffer was able to formulate a simple, convenient model including image effects [4]. He considered longitudinal beam dynamics directly without regard to the transverse dynamics. He did so by employing the geometry factor model for the beam's longitudinal electric fields. This model assumes that the longitudinal self-fields are proportional to the derivative of the line charge density of the beam, the proportionality constant being known as the geometry factor (or ''*g* factor''). Using the geometry factor Neuffer found that the parabolic line-charge density is a self-consistent solution to the equations of motion. He then derived a second-order differential equation for the longitudinal beam envelope of a bunched beam with parabolic line-charge density. This equation is extremely useful since one is able to study the longitudinal dynamics directly. However, for practical purposes we are then relegated to the determination of an appropriate geometry factor. Allen, Brown, and Reiser studied this geometry factor in detail [5]. They found, however, that the geometry factor model is not consistent with the actual fields generated by beam bunches. In order to circumvent this shortcoming, they proposed an average geometry factor which would be practical for back-of-the-envelope calculations. In the present paper the geometry factor is not considered. It is our aim to explicitly address the coupling between the radial and longitudinal motion, as well as the effects of images.

In previous works, image effects for continuous beams in cylindrical pipes were analyzed [6]. Here we extend the analysis for bunched beams in cylindrical pipes. We have studied bunched beam systems previously [5,7]; however, most of the results on beam dynamics were obtained numerically, and these conclusions were mainly qualitative. The current work is predominantly analytical, complementing the numerical work on image effects. Moreover, we derive a complete set of differential equations describing the evolution of the rms envelopes of bunched beams.

A. Equivalent beam concept

This work is essentially a continuation of the results of Sacherer [8]. He derived a set of coupled, ordinary differential equations that describe the evolution of the rms beam envelopes for continuous beams and bunched beams having ellipsoidal symmetry. In the continuous beam case, these equations have the same functional form as the Kapchinskij-Vladimirskij coupled-envelope equations [9] (KV equations). Indeed, for the uniform distribution these equations are the KV equations exactly. This fact has led to the notion of *equivalent beams*.

Sacherer's formalism allows us to model any continuous beam having elliptical symmetry with an equivalent KV

*Electronic address: cka@technosci.com
†Electronic address: mreiser@glue.umd.edu

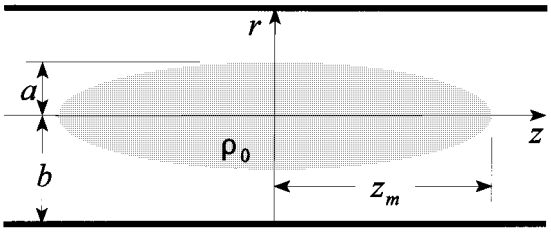

FIG. 1. Example bunch geometry of a uniform density ellipsoid.

beam (the KV beam is a uniform-density, continuous beam with elliptical cross-section). This equivalent beam must have the same second moments, or rms envelopes, as the actual beam under study. Thus, the KV coupled-envelope equations can be used to model any continuous beam with elliptical symmetry, as long as the rms beam envelopes are used in the equations. In this paper we address the question as to whether or not bunched beams might have the same properties. That is to say, is it possible to associate an equivalent beam to all bunched beams? And, if not, might there be certain parameter regimes where an approximation would hold true? We also consider this problem in the situation of a cylindrical, perfectly conducting beam pipe.

B. Ellipsoidal symmetry

As with Sacherer's analysis, we only consider bunched beams with ellipsoidal symmetry. Physically this condition means that the charge density of the bunch is constant along concentric ellipsoidal shells. This property also implies symmetry conditions with respect to all three Cartesian coordinate planes. The charge distribution is symmetric across the planes $x=0$, $y=0$, and $z=0$ (these coordinates are relative to the center of the bunch). These symmetry conditions allow a convenient mathematical description for the beam distribution.

Since we are primarily interested in the longitudinal dynamics, the analysis is further simplified by restricting our attention to the axisymmetric situation; the bunch has rotational symmetry around the beam axis. The results will still apply, in an average sense, to beams having eccentricity in the transverse plane. An example of our situation is shown in Fig. 1 for the uniform density distribution. The bunch is centered in the r-z coordinate plane, where r and z are cylindrical coordinates. It has density ρ_0 with a radial semiaxis a and an axial (longitudinal) semiaxis z_m.

C. Further limitations and assumptions

The major shortcoming of this work is that it does not describe a self-consistent situation. That is, we do not have complete coupling between the field quantities and the mechanics of the particle beam. The problem lies within the beam emittances. In this paper we must assume that the rms beam emittances are either constant or their variation is known *a priori*. The forehand knowledge of the rms emittances through the beam channel is usually an unrealistic expectation, since rms emittance growth is a complex phenoma, being difficult to model analytically. On the other hand, rms emittance growth usually occurs in the presence of nonlinear forces, and, from previous analysis [5], we know the image forces are typically nonlinear. Thus the assumption of constant emittances leaves us with a potentially inconsistent analysis.

So where does this leave us? The best possible course of action would seem to be the assumption of a stationary beam, that is, a beam whose distribution does not change in form over time. Therefore, the rms emittances would not change as well. There are several known stationary distributions, the KV (or microcanonical) distribution, the waterbag distribution, and the Maxwell-Boltzmann (or thermal) distribution, to name a few. Unfortunately, however, the ellipsoidal distribution is not one of them and we are back where we started.

We validate the results of this paper by considering the Maxwell-Boltzmann distribution, and noting a few practicalities. The Maxwell-Boltzmann distribution is probably the most important distribution from a practical standpoint, since it is the one seen most in experiments. First, assume that the focusing fields are linear, which is usually the situation. Then the two limiting cases of the Maxwell-Boltzmann distribution, the high-temperature and zero-temperature cases, are approximate ellipsoidal distributions. In the high-temperature case, where the self-fields become negligible compared to the applied fields, the distribution becomes Gaussian and ellipsoidally symmetric. Previous studies have shown that in the zero-temperature case the Maxwell-Boltzmann distribution is uniform and close to ellipsoidal in shape [7]. Since the Maxwell-Boltzmann distribution is stationary, the rms emittances would be approximately constant if one was operating close to one of these regimes. We cannot really predict the accuracy of the upcoming analysis whenever both emittance effects and space-charge effects are comparable.

The results of this paper are going to be the most useful and accurate for the space-charge-dominated case. This case is of primary importance for high-current applications, such as inertial fusion. The space-charge-dominated situation is the zero-temperature limiting case of the Maxwell-Boltzmann distribution. It is known that the charge density distributes itself almost uniformly (being exactly uniform at zero temperature), and that emittance (temperature) effects are negligible. Thus any unknown variations in the emittance would play little part in this situation. Moreover, we mentioned above that if the focusing fields are linear then the stationary distribution is close to ellipsoidal in shape. Thus, an accurate model for a space-charge-dominated bunched beam would be a uniform density ellipsoid. This case is considered in detail in this paper.

As our final precondition, we assume that the particle velocities relative to the (moving) bunch centroid are small enough so that magnetic field self-forces can be neglected. Thus the self-forces of the beam bunch are electrostatic in nature, and Poisson's equation is sufficient to describe them. Note, however, that the magnetic fields from the collective axial motion of the beam bunch are not neglected. These fields lead to the factor γ^2 in the rms envelope equations (γ being the relativistic factor).

D. Beam frame and local coordinates

The direction of propagation for charged particle beams is typically taken to be the z direction. However, we wish to

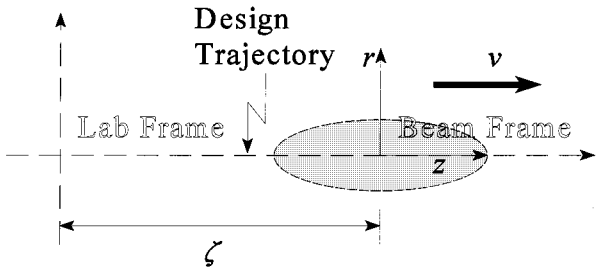

FIG. 2. The beam frame and the laboratory frame.

reserve the cylindrical coordinates (r,z) for points within the beam frame. Consequently, we introduce the path length parameter ζ which is the axial location (in the laboratory frame) of the bunch's center of mass. This parameter will serve as the independent variable, rather than time t.

We do not consider acceleration or the effects of acceleration. We assume that the beam coasts with an average axial velocity v. Therefore, the axial location ζ of the bunch centroid, starting at position $z=0$ after a time t, is given by $\zeta=vt$. Now we attach a coordinate system to the beam center which moves with velocity v along with the beam. We call this coordinate system the *beam frame*. Note that this frame is *not* the inertial frame of the beam, it is simply a laboratory frame coasting with the beam. The cylindrical coordinates (r,z) refer to points within the beam frame, called the *local coordinates*. The center of the beam frame (the bunch centroid) has coordinate $(r,z)=(0,0)$ and starts at the initial axial location of $\zeta=0$ at time $t=0$. The local coordinate z refers to the axial position of a particle with respect to the beam frame. Thus, a particle with local coordinates $(r,z)_{\text{beam}}$ in the beam frame has coordinates $(r,z+\zeta)_{\text{lab}}=(r,z+vt)_{\text{lab}}$ in the stationary laboratory frame. This situation is depicted in Fig. 2.

E. Density function

As mentioned, we consider beams with an ellipsoidal symmetry. To further simplify matters, we treat only the axisymmetric case, hence the use of cylindrical coordinates. For bunched beams this condition indicates that the particle density function n for the beam has the form

$$n(r,z)=f\left(\frac{r^2}{a^2}+\frac{z^2}{z_m^2}\right), \tag{1}$$

where f is some nonnegative real function. The quantities a and z_m are the semiaxes of concentric ellipsoids along which the density is constant, Fig. 1 illustrates these quantites for the example of a uniform ellipsoid. The quantities n, f, r, z, a, and z_m are all, in general, functions of ζ, however, we suppress this explicit dependence for ease of notion. From the above equation we find the beams's charge density ρ to be

$$\rho(r,z)=qn(r,z)=qf\left(\frac{r^2}{a^2}+\frac{z^2}{z_m^2}\right), \tag{2}$$

where q is the particle charge.

F. rms envelope equations

Denote by $\tilde{r}$ and $\tilde{z}$ the rms beam envelopes for the radial and axial directions, respectively. Denote the moment operator with respect to the particle distribution as $\langle\cdot\rangle$. Then $\tilde{r}$ and $\tilde{z}$ are defined as

$$\tilde{r}\equiv\langle r^2\rangle^{1/2} \quad \text{and} \quad \tilde{z}\equiv\langle z^2\rangle^{1/2}. \tag{3}$$

Using an analysis similar to that of Sacherer, we may derive a set of ordinary differential equations for the rms beam envelopes, they are [10]

$$\begin{aligned}\tilde{r}''+\kappa_r(\zeta)\tilde{r}-K\frac{2\pi\epsilon_0}{qN}\frac{\langle rE_r\rangle}{\tilde{r}}-\frac{\tilde{\epsilon}_r^{\,2}}{\tilde{r}^{\,3}}=0,\\ \tilde{z}''+\kappa_z(\zeta)\tilde{z}-\gamma^2K\frac{2\pi\epsilon_0}{qN}\frac{\langle zE_z\rangle}{\tilde{z}}-\frac{\tilde{\epsilon}_z^{\,2}}{\tilde{z}^{\,3}}=0,\end{aligned} \tag{4}$$

where $\kappa_r(\zeta)$ and $\kappa_z(\zeta)$ are the focusing functions in the radial and axial directions, E_r and E_z are the self-electric-field components in the radial and axial directions, $\tilde{\epsilon}_r$ and $\tilde{\epsilon}_z$ are the rms emittances in the radial and axial directions, respectively, γ is the relativistic factor given by $(1-v^2/c^2)^{1/2}$, K is the generalized beam perveance, N is the number of particles in the bunch, and ϵ_0 is the permittivity of free space. The perveance $K=(I/I_0)(2c^3/\gamma^3v^3)$, where I is the bunch current and I_0 is the characteristic current, is proportional to bunch charge Q since $I=Qv$. For a detailed description of these parameters, see Reiser [11]. The focusing functions $\kappa_r(\zeta)$ and $\kappa_z(\zeta)$ represent the external focusing system which contains the beam [e.g., a transport section, RFQ (radio frequency quadrupole), etc]. Thus, in the stationary beam situation, the quantities $\langle rE_r\rangle$ and $\langle rE_z\rangle$ are the only unknowns in the equations.

G. Definitions

Before proceeding, we introduce some definitions to simplify the foregoing analysis. First, let the integral of the density function f be given as g, specifically

$$g(r)\equiv\int_r^\infty f(s)ds. \tag{5}$$

Also, let the constant Γ be defined as

$$\Gamma\equiv\int_0^\infty g^2(r^2)dr. \tag{6}$$

The pth moment of the function f (and not of the function n) is denoted F_p; that is

$$F_p\equiv\int_0^\infty r^p f(r)dr. \tag{7}$$

We do not restrict the subscript p to integer values; for example, the number of bunch particles N may be expressed

$$N=2\pi\int_{-\infty}^{+\infty}\int_{0}^{+\infty}n(r,z)r\ dr\ dz$$
$$=2\pi\int_{-\infty}^{+\infty}\int_{0}^{+\infty}f\left(\frac{r^2}{a^2}+\frac{z^2}{z_m^2}\right)r\ dr\ dz$$
$$=2\pi a^2 z_m F_{1/2}, \tag{8}$$

where the final expression is obtained by integrating in polar coordinates. Finally, we define the quantities ξ and η as

$$\xi^2\equiv\frac{z_m^2-a^2}{z_m^2}=1-\frac{a^2}{z_m^2}=1-\frac{1}{2}\frac{\tilde{r}^{\,2}}{\tilde{z}^{\,2}}\quad(z_m>a),$$
$$\eta^2\equiv\frac{a^2-z_m^2}{z_m^2}=\frac{a^2}{z_m^2}-1=\frac{1}{2}\frac{\tilde{r}^{\,2}}{\tilde{z}^{\,2}}-1\quad(z_m<a). \tag{9}$$

The quantity ξ is known as the eccentricity of an ellipse with major axis z_m and minor axis a. It will appear quite frequently in the sequel.

II. FREE-SPACE RMS ENVELOPE EQUATIONS

The quantities $\langle rE_r\rangle$ and $\langle zE_z\rangle$ can be computed analytically in the free-space situation (i.e., no beam pipe). In this case the electric self-potential ϕ of the bunch is given by [2]

$$\phi(r,z)=\frac{qa^2z_m}{4\epsilon_0}\int_0^\infty\int_{S(t)}^\infty\frac{f(s)}{(a^2+t)(z_m^2+t)^{1/2}}\,ds\ dt, \tag{10}$$

where

$$S(t)\equiv\frac{r^2}{a^2+t}+\frac{z^2}{z_m^2+t}. \tag{11}$$

Using this expression, we find that [12]

$$\langle rE_r\rangle=\begin{cases}\dfrac{q}{4\epsilon_0}\dfrac{\Gamma}{F_{1/2}}\dfrac{a^2}{\xi^2}\left[1+\dfrac{\xi^2-1}{\xi}\operatorname{arctanh}\,\xi\right] & \text{for } z_m>a\\ \dfrac{q}{4\epsilon_0}\dfrac{\Gamma}{F_{1/2}}\dfrac{a^2}{\eta^2}\left[\dfrac{\eta^2+1}{\eta}\arctan\,\eta-1\right] & \text{for } z_m<a\end{cases} \tag{12}$$

and

$$\langle zE_z\rangle=\begin{cases}\dfrac{q}{4\epsilon_0}\dfrac{\Gamma}{F_{1/2}}\dfrac{a^2}{\xi^2}\left[\dfrac{1}{\xi\operatorname{arctanh}\,\xi}-1\right] & \text{for } z_m>a\\ \dfrac{q}{4\epsilon_0}\dfrac{\Gamma}{F_{1/2}}\dfrac{a^2}{\eta^2}\left[1-\dfrac{1}{\eta}\arctan\,\eta\right] & \text{for } z_m<a.\end{cases} \tag{13}$$

Substituting these expressions into Eqs. (4) yields the following set of differential equations for the rms envelopes $\tilde{r}$ and $\tilde{z}$:

$$\tilde{r}''+\kappa_r(\zeta)\tilde{r}-\Lambda(f)\frac{K}{\tilde{r}^{\,2}}W_r\left(\frac{\tilde{z}}{\tilde{r}}\right)-\frac{\tilde{\epsilon}_r^{\,2}}{\tilde{r}^{\,3}}=0,$$
$$\tilde{z}''+\kappa_z(\zeta)\tilde{z}-\Lambda(f)\frac{\gamma^2K}{\tilde{z}^{\,2}}W_z\left(\frac{\tilde{z}}{\tilde{r}}\right)-\frac{\tilde{\epsilon}_z^{\,2}}{\tilde{z}^{\,3}}=0, \tag{14}$$

where $\Lambda(f)$ is a positive function of the density function f defined by

$$\Lambda(f)\equiv\frac{1}{4\sqrt{3}}\frac{\Gamma[F_{3/2}]^{1/2}}{[F_{1/2}]^{5/2}}$$
$$=\frac{1}{4\sqrt{3}}\int_0^\infty g^2(r^2)dr\frac{[\int_0^\infty r^{3/2}f(r)dr]^{1/2}}{[\int_0^\infty r^{1/2}f(r)dr]^{5/2}}, \tag{15}$$

and the auxiliary functions $W_r(s)$ and $W_z(s)$ are defined as

$$W_r(s)\equiv\begin{cases}\dfrac{1}{2}\dfrac{1}{(\frac{1}{2}-s^2)^{3/2}}\arctan\dfrac{\sqrt{\frac{1}{2}-s^2}}{s}-\dfrac{s}{\frac{1}{2}-s^2} & \text{for } s\in[0,1/\sqrt{2})\\ \dfrac{s}{s^2-\frac{1}{2}}-\dfrac{1}{2}\dfrac{1}{(s^2-\frac{1}{2})^{3/2}}\operatorname{arctanh}\dfrac{\sqrt{s^2-\frac{1}{2}}}{s} & \text{for } s\in(1/\sqrt{2},\infty)\end{cases} \tag{16}$$

and

$$W_z(s)\equiv\begin{cases}\dfrac{s^2}{\frac{1}{2}-s^2}-\dfrac{s^3}{(\frac{1}{2}-s^2)^{3/2}}\arctan\dfrac{\sqrt{\frac{1}{2}-s^2}}{s} & \text{for } s\in(0,1/\sqrt{2})\\ \dfrac{s^3}{(s^2-\frac{1}{2})^{3/2}}\operatorname{arctanh}\dfrac{\sqrt{s^2-\frac{1}{2}}}{s}-\dfrac{s^2}{s^2-\frac{1}{2}} & \text{for } s\in(1/\sqrt{2},\infty).\end{cases} \tag{17}$$

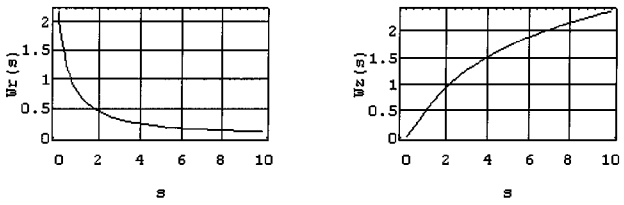

FIG. 3. Auxiliary functions $W_r(s)$ and $W_z(s)$.

The graphs of functions $W_r(s)$ and $W_z(s)$ are shown in Fig. 3. Equations (14) describe the evolution of the rms envelopes $\tilde{r}$ and $\tilde{z}$ as a function of position ζ.

Equivalent uniform bunched beam in free space

Notice that in the above situation the rms envelopes dynamics are dependent on the distribution. In Eqs. (14) the rms envelopes depend on the distribution through the function $\Lambda(f)$. If the form of the distribution remains constant during the evolution (for example, a uniform distribution or a Gaussian distribution), then $\Lambda(f)$ also remains constant. More importantly, however, referring to Table I we see that the value of $\Lambda(f)$ does not change significantly over a wide range of distributions. Consequently, in free space the dynamics are only loosely coupled to the form of the distribution, Sacherer pointed this out in his paper. Thus we may justify the the use of an equivalent beam for the bunched beam situation, which is approximately true in this case. Since it has well-defined beam envelopes, we take the uniform density ellipsoid (depicted in Fig. 1) to be our equivalent uniform beam in free space. The evolution of any bunched beam may be closely approximated with this uniform density ellipsoid having the same second moments as the actual bunch.

We derive the rms envelope equations for the equivalent uniform density beam in free space. For the uniform ellipsoidal distribution the function f has the form

$$f(x)=\begin{cases}\dfrac{3N}{4\pi a^2 z_m} & \text{for } x\leqslant 1\\ 0 & \text{for } x>1.\end{cases} \tag{18}$$

For this distribution note that a is the radial semiaxis of the bunch envelope, while z_m is the axial semiaxis. The constant value of the function f is seen to be the total number of particles divided by the volume of the ellipsoid. We compute the function $g(x)$ in Eq. (5) to be

$$g(x)=\begin{cases}\dfrac{3N}{4\pi a^2 z_m}(1-x) & \text{for } x\leqslant 1\\ 0 & \text{for } x>1.\end{cases} \tag{19}$$

From these expressions the value of $\Lambda(f)$ is

$$\Lambda(f)=\frac{3}{10\sqrt{5}}. \tag{20}$$

The rms envelopes for this distribution are given as

$$\tilde{r}\equiv\langle r^2\rangle^{1/2}=\sqrt{\tfrac{2}{5}}a,\quad \tilde{z}\equiv\langle z^2\rangle^{1/2}=\sqrt{\tfrac{1}{5}}z_m. \tag{21}$$

Note that the uniform density ellipsoid has a well-defined bunch envelope. Instead of writing differential equations for the rms beam envelopes $\tilde{r}$ and $\tilde{z}$, we may as well write them for the beam envelopes themselves. Such a set of equations would provide a more physical picture of the bunch dynamics. For the uniform density ellipsoid the quantities a and z_m are the bunch envelopes for the distribution. However, we wish to reserve these symbols for forthcoming calculations. We introduce the variables $R(\zeta)$ and $Z(\zeta)$ as the radial and axial envelopes (actually the semiaxes) for the uniform density ellipsoid. From Eqs. (21) the bunch envelopes are

$$R(\zeta)\equiv\sqrt{\tfrac{5}{2}}\tilde{r}\quad\text{and}\quad Z(\zeta)\equiv\sqrt{5}\tilde{z}. \tag{22}$$

We also introduce the effective emittances of the uniform density ellipsoid; these quantities are denoted ϵ_r and ϵ_z for the radial and axial directions, respectively. The effective emittances are

$$\epsilon_r\equiv\tfrac{5}{2}\tilde{\epsilon}_r\quad\text{and}\quad\epsilon_z\equiv 5\tilde{\epsilon}_z. \tag{23}$$

They normalize the differential equations for the bunch envelopes R and Z.

Collecting these results and substituting them into the moment equations of Sec. I yields

$$\begin{aligned}R''+\kappa_r(\zeta)R-\frac{3}{4\sqrt{5}}\frac{K}{R^2}W_r\left(\frac{Z}{\sqrt{2}R}\right)-\frac{\epsilon_r^2}{R^3}=0,\\ Z''+\kappa_z(\zeta)Z-\frac{3}{2}\frac{K}{Z^2}W_z\left(\frac{Z}{\sqrt{2}R}\right)-\frac{\epsilon_z^2}{Z^3}=0.\end{aligned} \tag{24}$$

These equations describe the behavior of the equivalent uniform density ellipsoid having the same second moments as the actual beam under study.

III. BEAM ENVELOPE EQUATIONS WITH IMAGE EFFECTS

Now we include the image effects in the dynamics equations. This is accomplished by including the contributions of the radial and axial image field components E_r^i and E_z^i when computing the moments $\langle rE_r\rangle$ and $\langle zE_z\rangle$. By linearity, we may simply add these contributions to those already obtained for the free-space situation. Thus, we need only compute the moments $\langle rE_r^i\rangle$ and $\langle zE_z^i\rangle$. Moreover, the image effects are negligible whenever the bunch is spherical or oblate [5]. Therefore, in the analysis to follow we only concern ourselves with the situation $z_m>a$, assuming that the image forces are zero otherwise.

We use a Green's function approach to find the fields E_r^i and E_z^i in the beam frame (recall that this is not an inertial frame). Specifically, the solution of Poisson's equation for the bunch potential $\phi(r,z)$ inside a conducting pipe with radius b is given by

$$\phi(r,z)=\int_{-\infty}^{+\infty}\int_0^b G(r,z;r_s,z_s)\rho(r_s,z_s)r_s dr_s dz_s, \tag{25}$$

where $G(r,z;r_s,z_s)$ is the Green's function, and $\rho(r_s,z_s)$ is the charge density of the beam bunch. Note that the cylindri-

TABLE I. Particle beam distributions and the corresponding $\Lambda(f)$. The symbols C and σ, respectively, represent the normalization constant and the standard deviation for the particular distribution.

Distribution	$f(x)$	$\Lambda(f)$	C
Uniform	C for $x\leqslant 1$ 0 for $x>1$	$\frac{3}{10}\frac{1}{\sqrt{5}}\approx 0.1342$	$\frac{3N}{4\pi a^2 z_m}$
Parabolic	$C(1-x)$ for $x\leqslant 1$ 0 for $x>1$	$\frac{5}{14}\frac{1}{\sqrt{7}}\approx 0.1350$	$\frac{15N}{8\pi a^2 z_m}$
Hollow	$Cxe^{-x/2\sigma^2}$	$\frac{1}{16}\left(\frac{15}{\pi}\right)^{1/2}\approx 0.1366$	$\frac{N}{3\sigma^5(2\pi)^{3/2}a^2 z_m}$
Gaussian	$Ce^{-x/2\sigma^2}$	$\frac{1}{4}\frac{1}{\sqrt{\pi}}\approx 0.1410$	$\frac{N}{\sigma^3(2\pi)^{3/2}a^2 z_m}$

cal coordinates (r,z) denote field points while (r_s,z_s) denotes source points. One representation for Green's function may be obtained by Fourier transforming the z coordinate in the Poission equation for an infinitesimal ring source. The result is [13]

$$G(r,z;r_s,z_s) = \frac{1}{2\pi\epsilon_0}\int_{-\infty}^{+\infty}\left(\frac{I_0(\omega b)K_0(|\omega|r_>)-I_0(\omega r_>)K_0(|\omega|b)}{I_0(\omega b)}\right) \times I_0(\omega r_<)e^{i\omega(z-z_s)}d\omega, \tag{26}$$

where I_0 and K_0 are the modified Bessel functions of the first and second kind, respectively, and $r_<\equiv\min(r,r_s)$ and $r_>\equiv\max(r,r_s)$. In this representation the free-space and image components may be readily identified. Note that $K_0(|x|)$ approaches zero and $I_0(x)$ blows up as x approaches infinity. Thus, taking the limit as b approaches infinity yields the free-space Green's function $G^f(r,z)$, given by

$$G^f(r,z;r_s,z_s)=\frac{1}{2\pi\epsilon_0}\int_{-\infty}^{+\infty}K_0(|\omega|r_>)I_0(\omega r_<)e^{i\omega(z-z_s)}d\omega. \tag{27}$$

This in turn implies that the image component of the Green's function, denoted $G^i(r,z)$, is given as

$$G^i(r,z;r_s,z_s)=-\frac{1}{2\pi\epsilon_0}\int_{-\infty}^{+\infty}\frac{K_0(|\omega|b)}{I_0(\omega b)}I_0(\omega r) \times I_0(\omega r_s)e^{i\omega(z-z_s)}d\omega. \tag{28}$$

Note that, unlike $G(r,z)$, the image component $G^i(r,z)$ is an analytic function of all of its arguments. We mention that an alternate form for G is obtained from a Bessel series expansion. It is given by [5]

$$G(r,z;r_s,z_s)=\frac{1}{\epsilon_0 b}\sum_{n=1}^{\infty}\frac{J_0(\beta_n r)J_0(\beta_n r_s)}{\alpha_n J_1^2(\alpha_n)}e^{-\beta_n|z-z_s|}. \tag{29}$$

A. Definitions

We pause here to introduce some more definitions. First, the Fourier transform operator is denoted $\mathcal{F}[\cdot]$ and a Fourier transformed function is indicated with the caret. (See Appendix B for a complete definition of the Fourier transform.) Thus we write $\hat{h}(\omega)=\mathcal{F}[h(x)]$ for the transform $\hat{h}(\omega)$ of the function $h(x)$.

In the sequel we encounter the Fourier transforms of certain expressions involving the functions f and g; we shall employ special notation for these quantities. Define the function $\tilde{f}(\omega)$ to be the Fourier transform of $x^2 f(x^2)$, that is,

$$\tilde{f}(\omega)\equiv\mathcal{F}[x^2 f(x^2)]=\int_{-\infty}^{+\infty}x^2 f(x^2)e^{-i\omega x}dx, \tag{30}$$

and define the function $\tilde{g}(\omega)$ to be the Fourier transform of $g(x^2)$,

$$\tilde{g}(\omega)\equiv\mathcal{F}[g(x^2)]=\int_{-\infty}^{+\infty}g(x^2)e^{-i\omega x}dx. \tag{31}$$

Note that the argument of both $f(x^2)$ and $g(x^2)$ is x^2 in the above definition. This makes f and g even functions of x and, therefore, the transforms $\tilde{f}(\omega)$ and $\tilde{g}(\omega)$ are both real, even functions of ω.

Also needed in the sequel will be the line-charge density of the distribution defined by f; this quantity is denoted $\rho_L(z)$. The line-charge density is found by integrating out the radial variation in $\rho(r,z)$; we have

$$\rho_L(z)\equiv 2\pi\int_0^{\infty}\rho(r,z)r\,dr=2\pi q\int_0^{\infty}f\left(\frac{2}{a^2}+\frac{z^2}{z_m^2}\right)r\,dr = q\pi a^2 g\left(\frac{z^2}{z_m^2}\right). \tag{32}$$

B. Image potential and image fields

The image potential ϕ^i for a bunch with ellipsoidal symmetry is expressed by substituting the Green's function of Eq. (28) into Eq. (25), and using the charge density of Eq. (2),

$$\phi^i(r,z) = -\frac{q}{2\pi\epsilon_0}\int_{-\infty}^{+\infty} d\omega\, \frac{K_0(|\omega|b)}{I_0(\omega b)}\, I_0(\omega r) e^{i\omega z} \times \int_{-\infty}^{+\infty}\int_0^{\infty} I_0(\omega r_s) e^{-i\omega z_s} f\left(\frac{r_s^2}{a^2}+\frac{z_s^2}{z_m^2}\right) r_s dr_s dz_s . \tag{33}$$

It is understood that the charge distribution is zero for all $r_s > b$, so the interval of integration over the coordinate r_s may be taken as $[0,\infty)$. We begin separating the integrations with the coordinate change $r_s = a\sigma_s(1-x_s^2)^{1/2}$ and $z_s = z_m\sigma_s x_s$ (which is a polar transform followed by $x_s = \cos\theta$),

$$\begin{aligned}\phi^i(r,z) &= -\frac{qa^2 z_m}{2\pi\epsilon_0}\int_{-\infty}^{+\infty} d\omega\, \frac{K_0(|\omega|b)}{I_0(\omega b)}\, I_0(\omega r) e^{i\omega z} \\ &\quad\times \int_{-1}^{+1}\int_0^{\infty} I_0\left(\omega a\sigma_s\sqrt{1-x_s^2}\right) e^{-i\omega z_m\sigma_s x_s} f(\sigma_s^2)\sigma_s^2 \\ &\quad\times d\sigma_s dx_s \\ &= -\frac{qa^2 z_m}{\pi\epsilon_0}\int_{-\infty}^{+\infty} d\omega\, \frac{K_0(|\omega|b)}{I_0(\omega b)}\, I_0(\omega r) e^{i\omega z} \\ &\quad\times \int_0^{1}\int_0^{\infty} I_0\left(\omega a\sigma_s\sqrt{1-x_s^2}\right) \cos(\omega z_m\sigma_s x_s) f(\sigma_s^2) \\ &\quad\times \sigma_s^2 d\sigma_s dx_s . \end{aligned} \tag{34}$$

In the second line we used the Euler representation for the cosine function to combine the integrations on either side of $x_s = 0$. Carrying out the integration over x_s (see Appendix A) yields

$$\phi^i(r,z) = -\frac{qa^2 z_m}{\pi\epsilon_0}\int_{-\infty}^{+\infty} d\omega\, \frac{K_0(|\omega|b)}{I_0(\omega b)}\, I_0(\omega r) e^{i\omega z} \times \int_0^{\infty} \mathrm{sinc}\left(\omega\sigma_s\sqrt{z_m^2-a^2}\right) f(\sigma_s^2)\sigma_s^2 d\sigma_s . \tag{35}$$

(See Appendix B for the definition of the sinc function.) This expression is only valid for $z_m > a$. Performing the integration over σ_s once by parts, we obtain

$$\phi^i(r,z) = -\frac{qa^2 z_m}{2\pi\epsilon_0}\int_{-\infty}^{+\infty} d\omega\, \frac{K_0(|\omega|b)}{I_0(\omega b)}\, I_0(\omega r) e^{i\omega z} \times \int_0^{\infty} g(\sigma_s^2)\cos\left(\omega\sigma_s\sqrt{z_m^2-a^2}\right) d\sigma_s . \tag{36}$$

Since σ_s^2 is an even function, $g(\sigma_s^2)$ is an even function over the interval $(-\infty,+\infty)$. With this in mind, we may consider the integration over σ_s to be a Fourier transform to the variable $\omega(z_m^2-a^2)^{1/2} = \omega\xi z_m$. Thus, the above equation may be interpreted as

$$\begin{aligned}\phi^i(r,z) &= -\frac{qa^2 z_m}{4\pi\epsilon_0}\int_{-\infty}^{+\infty} \frac{K_0(|\omega|b)}{I_0(\omega b)}\, I_0(\omega r)\widetilde{g}(\omega\xi z_m) e^{i\omega z} d\omega \\ &= -\frac{1}{2\pi\epsilon_0}\int_{-\infty}^{+\infty} \frac{K_0(|\omega|b)}{I_0(\omega b)}\, I_0(\omega r)\widetilde{\rho}_L(\xi\omega) e^{i\omega z} d\omega, \end{aligned} \tag{37}$$

where $\widetilde{g}$ is the Fourier transform of Eq. (31) and, in the second line, $\widetilde{\rho}_L$ is the Fourier transform of the line-charge density. The above equation for ϕ^i may be seen as an inverse Fourier transform.

From the expression for ϕ^i we can compute the fields components E_r^i and E_z^i by direct differentiation, we obtain

$$E_r^i(r,z) = \frac{qa^2 z_m}{4\pi\epsilon_0}\int_{-\infty}^{+\infty} \frac{K_0(|\omega|b)}{I_0(\omega b)}\, I_1(\omega r)\widetilde{g}(\omega\xi z_m) e^{i\omega z}\omega d\omega \tag{38}$$

and

$$E_z^i(r,z) = \frac{iqa^2 z_m}{4\pi\epsilon_0}\int_{-\infty}^{+\infty} \frac{K_0(|\omega|b)}{I_0(\omega b)}\, I_0(\omega r)\widetilde{g}(\omega\xi z_m) e^{i\omega z}\omega\, d\omega. \tag{39}$$

Note the imaginary coefficient i in the above equation indicates that E_z^i is an odd function of z.

It is also possible to compute the image charge on the pipe which is given by the surface-charge density $\sigma(z)$. This is done by comparing ϕ^i to the potential generated by $\sigma(z)$ in free space (i.e., the expression using G^f). We have [10]

$$\sigma(z) = -\frac{qa^2 z_m}{4\pi b}\int_{-\infty}^{+\infty} \frac{\widetilde{g}(\omega\xi z_m)}{I_0(\omega b)}\, e^{i\omega z} d\omega. \tag{40}$$

C. Image potential as an infinite summation

It is possible to express ϕ^i in terms of an infinite series of Bessel functions. We do this by considering Eq. (37) for ϕ^i as an inverse Fourier transform. Equation (37) may be rewritten as

$$\phi^i(r,z) = -\frac{1}{2\pi\epsilon_0}\int_{-\infty}^{+\infty} \hat{k}(r,\omega)\rho_L(\omega\xi z_m) e^{i\omega z} d\omega, \tag{41}$$

where

$$\hat{k}(r,\omega) \equiv K_0(|\omega|b)\,\frac{I_0(\omega r)}{I_0(\omega b)} \tag{42}$$

is the Fourier transform of some function $k(r,z)$, yet to be determined. Refering to Appendix B, we have

$$k(r,z) = \frac{1}{2}\frac{1}{\sqrt{r^2+z^2}} - \frac{1}{b}\sum_{n=1}^{\infty}\frac{J_0(\beta_n r)}{\alpha_n J_1^2(\alpha_n)}\, e^{-\beta_n|z|}. \tag{43}$$

Using the convolution theorem [14] for Fourier transforms, we may transform the integration over the ''spatial fre-

quency'' parameter ω into a convolution over the source's spatial coordinate z_s. An application of the convolution theorem yields

$$\phi^i(r,z) = -\frac{1}{2\pi\epsilon_0}\int_{-\infty}^{+\infty} k(r,z,-z_s)\,\frac{1}{\xi}\,\rho_L\left(\frac{z_s}{\xi}\right)dz_s . \tag{44}$$

Substituting in the expression for $k(r,z)$ yields

$$\phi^i(r,z) = -\frac{1}{4\pi\epsilon_0}\int_{-\infty}^{+\infty}\frac{\frac{1}{\xi}\,\rho_L\left(\frac{z_s}{\xi}\right)}{[r^2+(z-z_s)^2]^{1/2}}\,dz_s + \frac{1}{2\pi\epsilon_0 b} \times\sum_{n=1}^{\infty}\frac{J_0(\beta_n r)}{\alpha_n J_1^2(\alpha_n)}\int_{-\infty}^{+\infty}\frac{1}{\xi}\,\rho_L\left(\frac{z_s}{\xi}\right)e^{-\beta_n|z+z_s|}dz_s . \tag{45}$$

The image fields behave as though they are due to a line charge obtained by uniformly contracting $\rho_L(z)$ by a factor ξ. The first term is the negation of free-space potential outside the charge distribution (this quantity may be computed directly). The second term is the full potential (both image and free space) from the line-charge distribution $\rho_L(z/\xi)/\xi$ centered in a perfectly conducting pipe with radius b, as interpreted from the alternate representation for Green's function of Eq. (29). This situation is depicted schematically in Fig. 4 for a bunch with eccentricity $\xi=(1-a^2/z_m^2)^{1/2}$. Thus, outside the distribution, the total fields for a bunch behave as though they are generated by the line charge $\rho_L(z/\xi)/\xi$.

The surface-charge density $\sigma(z)$ may also be found in terms of an infinite series of Bessel functions using a similar procedure. Proceeding in an analogous manner, we find

$$\sigma(z) = -\frac{1}{2\pi b^2}\sum_{n=1}^{\infty}\frac{1}{J_1(\alpha_n)}\int_{-\infty}^{+\infty}\frac{1}{\xi}\,\rho_L\left(\frac{z_s}{\xi}\right)e^{-\beta_n|z-z_s|}dz_s . \tag{46}$$

The image charge also seems to be induced by the line-charge distribution $\rho_L(z/\xi)/\xi$.

D. Image components of $\langle rE_r\rangle$ and $\langle zE_z\rangle$

Now consider the moments $\langle rE_r^i\rangle$ and $\langle zE_z^i\rangle$, which are the respective contributions to $\langle rE_r\rangle$ and $\langle zE_z\rangle$ from the image charge on the pipe. The integrations occurring in these computations may be separated with coordinate transformations similar to those used to compute ϕ^i. This time, however, they are applied to the field coordinates (r,z). First we concentrate on the moment $\langle zE_z^i\rangle$,

$$\begin{aligned}\langle zE_z^i\rangle &= \frac{iqa^2z_m}{2\epsilon_0 N}\int_{-\infty}^{+\infty}d\omega\;\omega\,\frac{K_0(|\omega|b)}{I_0(\omega b)}\,\tilde{g}(\omega\xi z_m)\int_{-\infty}^{+\infty}\int_0^{\infty}I_0(\omega r)e^{i\omega z}f\left(\frac{r^2}{a^2}+\frac{z^2}{z_m^2}\right)zr\;dr\;dz\\ &= \frac{iqa^4z_m^3}{2\epsilon_0 N}\int_{-\infty}^{+\infty}d\omega\;\omega\,\frac{K_0(|\omega|b)}{I_0(\omega b)}\,\tilde{g}(\omega\xi z_m)\int_0^{\infty}d\sigma\;f(\sigma^2)\sigma^3\int_{-1}^{1}xI_0(\omega a\sigma\sqrt{1\text{-}x^2})e^{i\omega z_m\sigma x}dx,\end{aligned} \tag{47}$$

where we have again used the change of coordinates $r=a\sigma(1-x^2)^{1/2}$ and $z=z_m\sigma x$ in the second line. Note that the integrand, less the complex exponent, is an odd function of x. Thus the complex exponent may be converted to a sine function by changing the interval of integration to (0,1]. We also obtain a factor $2i$ from the Euler representation of the sine function. The result is

$$\begin{aligned}\langle zE_z^i\rangle &= \frac{iqa^4z_m^3}{2\epsilon_0 N}\int_{-\infty}^{+\infty}d\omega\;\omega\,\frac{K_0(|\omega|b)}{I_0(\omega b)}\,\tilde{g}(\omega\xi z_m)\\ &\times\int_0^{\infty}d\sigma\;\sigma^3 f(\sigma^2)2i\int_0^1 xI_0(\omega a\sigma\sqrt{1-x^2})\\ &\times\sin(\omega z_m\sigma x)dx.\end{aligned} \tag{48}$$

We may now carry out the integration over x by referring to Appendix A. The result is

$$\begin{aligned}\langle zE_z^i\rangle &= -\frac{qa^4z_m^3}{\epsilon_0 N}\int_{-\infty}^{+\infty}d\omega\;\omega\,\frac{K_0(|\omega|b)}{I_0(\omega b)}\,\tilde{g}(\omega\xi z_m)\\ &\times\frac{z_m}{\omega(z_m^2-a^2)}\int_0^{\infty}\sigma^2 f(\sigma^2)\Big(\operatorname{sinc}\omega\sigma\sqrt{z_m^2-a^2}\\ &-\cos\omega\sigma\sqrt{z_m^2-a^2}\Big)d\sigma,\end{aligned} \tag{49}$$

which is technically valid only for the case $z_m>a$. If we interpret the integration over σ as a Fourier transform to the

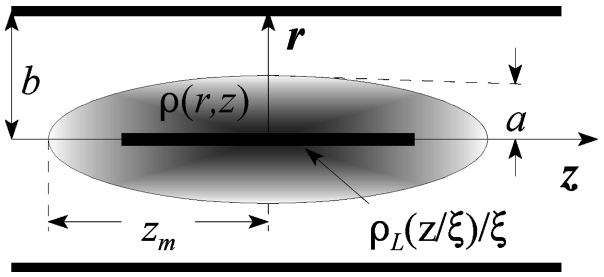

FIG. 4. Beam bunch and its equivalent image field source.

variable $\omega(z_m^2-a^2)^{1/2}=\omega\xi z_m$, as we did in the expression for ϕ^i, the above expression becomes

$$\langle zE_z^i\rangle=-\frac{qa^4z_m}{2\epsilon_0N\xi^3}\int_{-\infty}^{+\infty}\frac{K_0\left(|\omega|\dfrac{b}{\xi z_m}\right)}{I_0\left(\omega\dfrac{b}{\xi z_m}\right)}\times[\tfrac{1}{2}\tilde{g}(\omega)\tilde{g}(\omega)-\tilde{f}(\omega)g(\omega)]d\omega, \tag{50}$$

where we have used the substitution $\omega\rightarrow\omega\xi z_m$.

Now consider the moment $\langle rE_r^i\rangle$. Proceeding in a fashion similar to that for the moment $\langle zE_z^i\rangle$, the moment $\langle rE_r^i\rangle$ is represented as

$$\langle rE_r^i\rangle=\frac{qa^5z_m^2}{2\epsilon_0N}\int_{-\infty}^{\infty}d\omega\ \omega\ \frac{K_0(|\omega|b)}{I_0(\omega b)}\tilde{g}(\omega\xi z_m)\times\int_0^{\infty}d\sigma\ \sigma^3f(\sigma^2)\int_{-1}^{1}\sqrt{1-x^2}I_1(\omega a\sigma\sqrt{1-x^2})\times e^{i\omega z_m\sigma x}dx. \tag{51}$$

The term $(1-x^2)^{1/2}$ in the integration over x arises from the factor r in the quantity $\langle rE_r^i\rangle$, it is analogous to the factor x which appears in the expression for $\langle zE_z^i\rangle$. The integration over x may be simplified by performing one integration by parts to yield

$$\langle rE_r^i\rangle=\frac{qa^6z_m}{2i\epsilon_0N}\int_{-\infty}^{+\infty}d\omega\ \omega\ \frac{K_0(|\omega|b)}{I_0(\omega b)}\tilde{g}(\omega\xi z_m)\times\int_0^{\infty}d\sigma\ \sigma^3f(\sigma^2)\int_{-1}^{1}xI_0(\omega a\sigma\sqrt{1-x^2})e^{i\omega z_m\sigma x}dx. \tag{52}$$

The integration over x may now be carried out (again, using Appendix A) to find the expression

$$\langle rE_r^i\rangle=\frac{4qa^6z_m^2}{\epsilon_0N(z_m^2-a^2)}\int_{-\infty}^{+\infty}d\omega\ \frac{K_0(\omega b)}{I_0(\omega b)}\tilde{g}(\omega\xi z_m)\times\int_0^{\infty}\sigma^2f(\sigma^2)\left(\operatorname{sinc}\omega\sigma\sqrt{z_m^2-a^2}-\cos\omega\sigma\sqrt{z_m^2-a^2}\right)d\sigma. \tag{53}$$

In terms of the Fourier transforms $\tilde{f}$ and $\tilde{g}$, this moment may be expressed as

$$\langle rE_r^i\rangle=\frac{qa^6}{2\epsilon_0N\xi^3z_m}\int_{-\infty}^{+\infty}\frac{K_0\left(|\omega|\dfrac{b}{\xi z_m}\right)}{I_0\left(\omega\dfrac{b}{\xi z_m}\right)}\times[\tfrac{1}{2}\tilde{g}(\omega)\tilde{g}(\omega)-\tilde{f}(\omega)\tilde{g}(\omega)]d\omega. \tag{54}$$

The final expressions for $\langle rE_r^i\rangle$ and $\langle zE_z^i\rangle$ cannot be further reduced without an *a priori* knowledge of the distribution f. However, once the distribution f is chosen the integrations in the expressions for $\langle rE_r^i\rangle$ and $\langle zE_z^i\rangle$ have only one parameter. This condition facilitates the introduction of an auxiliary function $A_f(x)$, defined

$$A_f(x)\equiv C_A\int_{-\infty}^{\infty}\frac{K_0(\omega x)}{I_0(\omega x)}\tilde{g}(\omega)[\tfrac{1}{2}\tilde{g}(\omega)-\tilde{f}(\omega)]d\omega. \tag{55}$$

The factor C_A is added to provide some normalization, we shall choose

$$C_A=\frac{2\pi^2a^4z_m^2}{9N^2}, \tag{56}$$

which favors the uniform density distribution. The image components can be written in terms of the function A_f,

$$\langle rE_r^i\rangle=\frac{1}{C_A}\frac{qa^6}{2\epsilon_0N\xi^3z_m}A_f\left(\frac{b}{\xi z_m}\right)=\frac{9Q}{4\pi^2\epsilon_0}\frac{a^2}{\xi^3z_m^3}A_f\left(\frac{b}{\xi z_m}\right) \tag{57}$$

and

TABLE II. Particle beam distributions and their corresponding $A_f(x)$.

Distribution	$A_f(x)$.
Uniform	$\displaystyle\int_{-\infty}^{+\infty}\frac{K_0(\lvert\omega\rvert x)}{I_0(\omega x)}\left(\frac{3\cos\omega}{\omega^2}-\frac{3\operatorname{sinc}\omega}{\omega^2}+\operatorname{sinc}\omega\right)\left(\frac{\cos\omega}{\omega^2}-\frac{\operatorname{sinc}\omega}{\omega^2}\right)d\omega$
Parabolic	$\displaystyle\frac{225}{9}\int_{-\infty}^{+\infty}\frac{K_0(\lvert\omega\rvert x)}{I_0(\omega x)}\left(\frac{3\cos\omega}{\omega^4}-\frac{3\operatorname{sinc}\omega}{\omega^4}+\frac{\operatorname{sinc}\omega}{\omega^2}\right)\left(\frac{15\cos\omega}{\omega^4}-\frac{15\operatorname{sinc}\omega}{\omega^4}-\frac{\cos\omega}{\omega^2}+\frac{6\operatorname{sinc}\omega}{\omega^2}\right)d\omega$
Hollow	$\displaystyle\frac{1}{81}\int_{-\infty}^{+\infty}\frac{K_0(\lvert\omega\rvert x)}{I_0(\omega x)}\omega^2(\omega^2-3)(\omega^2-5)e^{-\omega^2}d\omega$
Gaussian	$\displaystyle\frac{1}{9}\int_{-\infty}^{+\infty}\frac{K_0(\omega x)}{I_0(\omega x)}\omega^2e^{-\omega^2}d\omega$

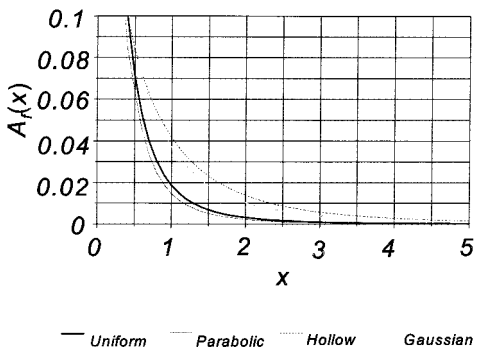

FIG. 5. Comparison of the image effects function $A_f(x)$ for four different distributions.

$$\langle zE_z^i\rangle = -\frac{1}{C_f}\frac{qa^4 z_m}{2\epsilon_0 N\xi^3}A_f\left(\frac{b}{\xi z_m}\right) = -\frac{Q}{4\pi^2\epsilon_0}\frac{z_m^2}{\xi^3 z_m^3}A_f\left(\frac{b}{\xi z_m}\right), \tag{58}$$

where $Q=qN$ is the total bunch charge.

E. Beam envelope equations with image effects

The expressions for moments $\langle rE_r^i\rangle$ and $\langle zE_z^i\rangle$ are added to the free-space moments $\langle rE_r\rangle$ and $\langle zE_z\rangle$ to form the complete moments. Referring to the differential set of Eq. (24) for the equivalent uniform ellipsoid, the image effects are included directly by adding the image components to the space-charge terms. The result is

$$\begin{aligned} R''+\kappa_r(\zeta)R-\frac{3K}{4\sqrt{5}}\frac{1}{R^2}W_r\left(\frac{Z}{\sqrt{2}R}\right) \\ -\frac{45K}{2}\frac{R}{(Z^2-R^2)^{3/2}}A_f\left(\frac{b}{\sqrt{Z^2-R^2}}\right)-\frac{\epsilon_r^2}{R^3}=0, \\ Z''+\kappa_z(\zeta)Z-\frac{3\gamma^2K}{2}\frac{1}{Z^2}W_z\left(\frac{Z}{\sqrt{2}R}\right) \\ +\frac{45\gamma^2K}{2}\frac{Z}{(Z^2-R^2)^{3/2}}A_f\left(\frac{b}{\sqrt{Z^2-R^2}}\right)-\frac{\epsilon_z^2}{Z^3}=0. \end{aligned} \tag{59}$$

These equations describe the envelope dynamics of the equivalent uniform density ellipsoid inside a beam pipe. Note, however, that these equations are dependent upon the particle distribution through the function A_f. Thus, to determine whether or not there is an equivalent distribution, we need to explore the dependency of A_f on f.

F. Analysis of the function A_f for different distributions

Here we explore the behavior of $A_f(x)$ for several different particle distributions to determine its dependency upon the distribution. Table II lists the integral expressions of $A_f(x)$ for the distributions originally presented in Table I. The integrations were computed numerically, and their corresponding graphs are shown in Fig. 5. The most important curves in the figure are probably those of the uniform distribution, and the Gaussian distributions since they represent the two extreme cases of the Maxwell-Boltzmann (or thermal) distribution. Note that from this graph it can be seen that the image effects are most significant for $x<1$, corresponding to the long-bunch case where $Z\gg R$. Here the uniform distribution has the most significant image effects. We see from Fig. 5 that we really do not have an equivalent beams principle for the bunched beam case. One should use the function $A_f(x)$ for the distribution closest to that of the actual beam under study. Since many practical beams have Maxwell-Boltzmann distributions, we can expect the function $A_f(x)$ for these beams to lie somewhere between that of the uniform distribution and the Gaussian distribution. In the remainder of this paper we continue the analysis using the uniform distribution with the intent of modeling the space-charge-dominanted situation.

IV. UNIFORM DENSITY ELLIPSOID

It is possible to derive analytic expressions for the quantities of interest in terms of infinite series of Bessel functions. In particular, we derive an expression the function $A_f(x)$, for the uniform density ellipsoid having a radial semiaxis a and an axial semiaxis z_m. We list several other results of interest before proceeding to the calculation of $A_f(x)$. In particular, expressions for the image potential and image charge are derived. The expressions in this section mostly of analytic value, since all contain infinite summations of Bessel functions. However, we used asymptotic expressions for $A_f(x)$ which were derived from Eq. (69) when numerically solving the differential system in Eqs. (59).

A. Image potential and image charge

The image potential ϕ^i in for the uniform distribution is found by substituting Eq. (18) into Eq. (32), and then into Eq. (44). After integrating we have

$$\begin{aligned} \phi^i(r,z) = \frac{3Q}{32\pi\epsilon_0\xi^3 z_m^3}\left[(\xi z_m-3z)\sqrt{r^2+(z+\xi z_m)^2}+(\xi z_m+3z)\sqrt{r^2+(z-\xi z_m)^2}\right] \\ +\frac{3Q}{16\pi\epsilon_0\xi z_m}\left[\left(1+\frac{r^2}{2\xi^2 z_m^2}-\frac{z^2}{\xi^2 z_m^2}\right)\ln\left(\frac{-z-\xi z_m+\sqrt{r^2+(z+\xi z_m)^2}}{-z+\xi z_m+\sqrt{r^2+(z-\xi z_m)^2}}\right)\right]+\frac{3Q}{4\pi\epsilon_0\xi z_m}\sum_{n=1}^{\infty}\frac{J_0(\beta_n r)}{\alpha_n^2 J_1^2(\alpha_n)}B_n(z), \end{aligned} \tag{60}$$

where the auxiliary function $B_n(z)$ is defined by

$$B_n(z)\equiv\begin{cases}\left(1-\dfrac{z^2}{\xi^2 z_m^2}\right)+\dfrac{2e^{-\beta_n\xi z_m}\cosh(\beta_n z)}{\beta_n\xi z_m}+\dfrac{2e^{-\beta_n\xi z_m}\cosh(\beta_n z)-2}{\beta_n^2\xi^2 z_m^2} & \text{for } z\in[-\xi z_m,+\xi z_m]\\ \dfrac{2e^{-\beta_n|z|}\cosh(\beta_n\xi z_m)}{\beta_n\xi z_m}-\dfrac{2e^{-\beta_n|z|}\sinh(\beta_n\xi z_m)}{\beta_n^2\xi^2 z_m^2} & \text{for } |z|>\xi z_m .\end{cases} \tag{61}$$

We see that the fringe fields for the image charge seem to be located around $z=\pm\xi z_m$.

The logarithmic term in Eq. (60) contains a singularity at $r=0$ whenever $z\in[-\xi z_m,+\xi z_m]$, since its argument approaches zero as r approaches zero. Physically, we know that the image potential is well behaved along the z axis. Thus, the Bessel summation must contain an opposing singularity to cancel that of the logarithmic term. It is possible to identify this singularity and, consequently, obtain a numerically stable expression. The axial ($r=0$) image potential is given as (again see Allen [10] for details)

$$\phi^i(0,z)=\frac{3Q}{16\pi\epsilon_0\xi z_m}\times\begin{cases}1-\dfrac{3z^2}{\xi^2 z_m^2}+\left(1-\dfrac{z^2}{\xi^2 z_m^2}\right)\ln\left(\dfrac{1}{4}\dfrac{b^2}{\xi^2 z_m^2-z^2}\right)+\displaystyle\sum_{n=1}^{\infty}\frac{4B_n^i(z)}{\alpha_n^2 J_1^2(\alpha_n)} & \text{for } |z|<\xi z_m\\ -2\dfrac{|z|}{\xi z_m}\pm\left(1-\dfrac{z^2}{\xi^2 z_m^2}\right)\ln\left(\dfrac{|z-\xi z_m|}{|z+\xi z_m|}\right)+\displaystyle\sum_{n=1}^{\infty}\frac{4B_n^o(z)}{\alpha_n^2 J_1^2(\alpha_n)} & \text{for } |z|\geqslant\xi z_m ,\end{cases} \tag{62}$$

where choice of the sign in the second line depends on which side of zero z lies ($+$ for $z>0$ and $-$ for $z<0$), and the two auxiliary functions $B_n^i(z)$ and $B_n^o(z)$ are defined

$$B_n^i(z)\equiv\frac{2e^{-\beta_n\xi z_m}\cosh(\beta_n z)}{\beta_n\xi z_m}+\frac{2e^{-\beta_n\xi z_m}\cosh(\beta_n z)-2}{\beta_n^2\xi^2 z_m^2},$$

$$B_n^o(z)\equiv\frac{2e^{-\beta_n|z|}\cosh(\beta_n\xi z_m)}{\beta_n\xi z_m}-\frac{2e^{-\beta_n|z|}\sinh(\beta_n\xi z_m)}{\beta_n^2\xi^2 z_m^2}. \tag{63}$$

In the long bunch limit ($z_m\to\infty$) B_n^i and B_n^o approach zero, indicating that these quantities represent the fringe fields of the bunch. The free-space potential for the uniform ellipsoid has previously been determined [1]. One may add that expression to the above to obtain the full potential for a uniform density ellipsoid in a cylindrical pipe.

Now consider the induced surface-charge density $\sigma(z)$ on the beam pipe. This quantity is found by first substituting Eq. (18) into Eq. (32) to find $\rho_L(z)$ for the uniform ellipsoid. Then substitute this value into Eq. (46), which can be integrated with the result

$$\sigma(z)=\frac{-3Q}{4\pi b\xi z_m}\sum_{n=1}^{\infty}\frac{1}{\alpha_n J_1(\alpha_n)}\times\begin{cases}1-\dfrac{z^2+2/\beta_n^2}{\xi^2 z_m^2}+\left(\dfrac{2}{\beta_n\xi z_m}+\dfrac{2}{\beta_n^2\xi^2 z_m^2}\right)e^{-\beta_n\xi z_m}\cosh\beta_n z & \text{for } |z|\leqslant\xi z_m\\ \left(\dfrac{2\cosh\beta_n z_m}{\beta_n\xi z_m}-\dfrac{2\sinh\beta_n z_m}{\beta_n^2\xi^2 z_m^2}\right)e^{-\beta_n z} & \text{for } |z|>\xi z_m .\end{cases} \tag{64}$$

This expression can be simplified somewhat by identifying some of the convergent Bessel summations in the above (again, see Allen [10]). Doing so yields

$$\sigma(z)=\frac{-3Q}{8\pi b\xi z_m}\times\begin{cases}1-\dfrac{z^2}{\xi^2 z_m^2}-\dfrac{b^2}{2\xi^2 z_m^2}+\displaystyle\sum_{n=1}^{\infty}\frac{4e^{-\beta_n\xi z_m}\cosh\beta_n z}{\alpha_n J_1(\alpha_n)}\left(\dfrac{1}{\beta_n\xi z_m}+\dfrac{1}{\beta_n^2\xi^2 z_m^2}\right) & \text{for } |z|\leqslant\xi z_m\\ \displaystyle\sum_{n=1}^{\infty}\frac{4e^{-\beta_n|z|}}{\alpha_n J_1(\alpha_n)}\left(\dfrac{\cosh\beta_n z_m}{\beta_n\xi z_m}-\dfrac{\sinh\beta_n z_m}{\beta_n^2\xi^2 z_m^2}\right) & \text{for } |z|>\xi z_m .\end{cases} \tag{65}$$

Thus, the image charges on the pipe are mostly parabolic with some exponential decay. Since the Bessel series approaches zero in the long bunch limit, the image charge would be parabolic in the region $z \in [-\xi z_m, +\xi z_m]$, and zero elsewhere.

B. Image effects function

For clarity the image effects function $A_f(x)$ for the uniform ellipsoid will henceforth be denoted simply as $A(x)$. We now transform the expression for $A(x)$ in Table II to an infinite summation representation. This is accomplished by using Parseval's theorem [14], and realizing the following fact:

$$\begin{aligned}\mathcal{F}^{-1}[\hat{k}(0,\omega)\hat{g}(\omega\xi z_m)] &= \frac{1}{2\pi}\int_{-\infty}^{+\infty} \frac{K_0(|\omega|b)}{I_0(\omega b)}\,\hat{g}(\omega\xi z_m) \\ &\quad \times e^{i\omega z} d\omega \\ &= -\frac{1}{2\pi}\frac{4\pi\epsilon_0}{qa^2 z_m}\,\phi^i(0,z). \end{aligned} \tag{66}$$

Thus, in general, the function $A_f(x)$ may be expressed as

$$A_f(x) = C_f \int_{-\infty}^{+\infty} [\hat{k}(0,\omega)_x^b \hat{g}(\omega\xi z_m)_{1/z_m}^{\xi}][\hat{g}(\omega) - \tfrac{1}{2}\hat{f}(\omega)]\,d\omega, \tag{67}$$

where the notation $\tilde{k}(0,\omega)_x^b$ means to replace all occurrences of b in $\tilde{k}(0,\omega)$ with x. Note that the substitution operators $|_x^b$ and $|_x^{\xi}$ commute with the integration. An application of Parseval's theorem to the factors in square brackets transforms the above to

$$\begin{aligned} A_f(x) &= -\frac{4\pi\epsilon_0}{qa^2 z_m}\, C_f \int_{-\infty}^{+\infty} [\phi^i(0,z)_{x,1/z_m}^{b,\xi}] \\ &\quad \times [\tfrac{1}{2}g(z^2) - z^2 f(z^2)]\,dz. \end{aligned} \tag{68}$$

Note that this is a general expression and is valid for all distributions, hence the notation $A_f(x)$. Now we concentrate on the uniform distribution.

Into the above equation we substitute Eq. (62) for ϕ^i and insert the expressions of $f(z^2)$ and $g(z^2)$ for the uniform distribution. This action leaves us with an integral expression for $A(x)$ which may be evaluated analytically. The result is

$$A(x) = -\frac{61\pi}{450} - \frac{\pi}{15}\ln\left(\frac{x}{4}\right) + 2\pi\Xi_A(x), \tag{69}$$

where the function $\Xi_A(x)$ is defined

$$\begin{aligned}\Xi_A(x) \equiv \sum_{n=1}^{\infty} &\frac{1}{\alpha_n^2 J_1^2(\alpha_n)}\left(\frac{x}{\alpha_n} + \frac{x^2}{\alpha_n^2}\right)\left(\frac{x}{\alpha_n}\sinh\frac{\alpha_n}{x}\right. \\ &\left. - \frac{3x^2}{\alpha_n^2}\cosh\frac{\alpha_n}{x} + \frac{3x^3}{\alpha_n^3}\sinh\frac{\alpha_n}{x}\right) e^{-\alpha_n/x}. \end{aligned} \tag{70}$$

From Eq. (69) and the fact that $\Xi_A(0) = 0$ we see that $A(x)$ behaves logarithmically around $x = 0$. For large values of x we see, from Eq. (55), that $A(x)$ approaches zero, so that $\Xi_A(x)$ behave logarithmically to cancel the negative logarithm in Eq. (69).

C. Beam envelope equations

As argued in Sec. I, for the space-charge-dominated situation a bunched beam may be accurately modeled by a uniform ellipsoid. Mathematically this is represented by the system described by Eqs. (59), (16), (17), and (69). We collect these results below for convenience.

$$\begin{aligned} &R'' + \kappa_r(\zeta)R - \frac{3K}{4\sqrt{5}}\frac{1}{R^2}\,W_r\left(\frac{Z}{\sqrt{2}R}\right) \\ &\quad - \frac{45K}{2}\frac{R}{(Z^2-R^2)^{3/2}}\,A(R,Z) - \frac{\epsilon_r^2}{R^3} = 0, \\ &Z'' + \kappa_z(\zeta)Z - \frac{3\gamma^2 K}{2}\frac{1}{Z^2}\,W_z\left(\frac{Z}{\sqrt{2}R}\right) \\ &\quad + \frac{45\gamma^2 K}{2}\frac{Z}{(Z^2-R^2)^{3/2}}\,A(R,Z) - \frac{\epsilon_z^2}{Z^3} = 0, \end{aligned} \tag{71}$$

where the new representation for the image function A is given as

$$A(R,Z) \equiv \begin{cases} A\left(\dfrac{b}{\sqrt{Z^2-R^2}}\right) & \text{for } Z > R \\ 0 & \text{for } Z < R\,. \end{cases} \tag{72}$$

The above result is taken from Eq. (69), and the fact that image effects are negligible whenever $Z < R$. Once a table of values for $A(x)$ is constructed (for interpolation), this system may be easily integrated using standard numerical techniques.

D. A simple example

To illustrate the utility of these results, we simulated a simple transport system for bunched particle beams. The transport system has uniform focusing in the radial direction and period focusing in the longitudinal direction. The focusing functions for both directions is shown in Fig. 6(a). Note that we have used a ''hard-edge'' approximation for the function $\kappa_z(\zeta)$. The period of $\kappa_z(\zeta)$ is 25 cm, the pulse length being 5 cm, with a maximum value 200 m^{-2}. The constant value of $\kappa_r(\zeta)$ is 100 m^{-2}. The beam parameters are given as follows: $K = 0.01$, $\epsilon_r = 5\times10^{-5}$ m rad, $\epsilon_z = 2\times10^{-5}$ m rad, and $\gamma = 1$.

The function $A(x)$ was constructed by numerically computing values for x in the interval [0.3,6.3]. These values were tabulated in order to interpolate $A(x)$ for all the values of x in this range. Asymptotic expressions derived from Eq. (69) were used for $x < 0.3$, and we took $A(x) = 0$ for $x > 6.3$.

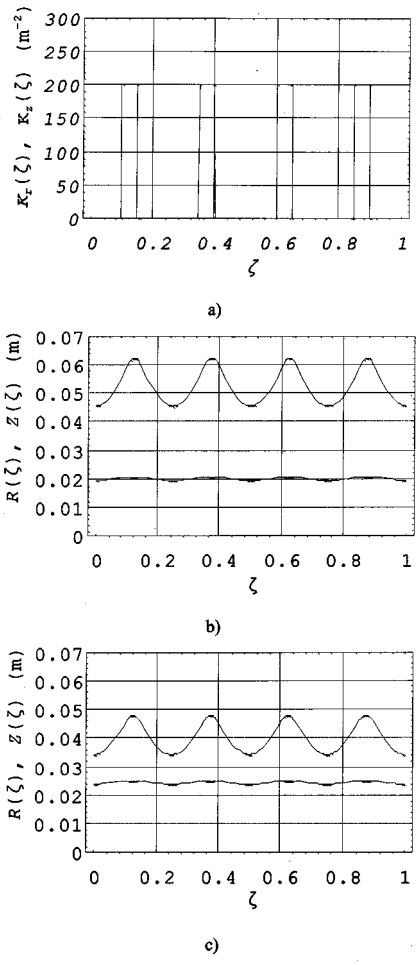

FIG. 6. Example solutions (a) the focusing functions, (b) the matched beam solution for the free-space situation, and (c) the matched beam solution with image effects.

The matched beam solution in free space is shown in Fig. 6(b), while the matched beam solution including a pipe with radius $b=5$ cm is shown in Fig. 6(c). Without the beam pipe, the minimum radial and longitudinal matched beam envelopes are $R_0=1.94$ cm and $Z_0=4.54$ cm, respectively. With the beam pipe the values are $R_0=2.39$ cm and $Z_0=3.43$ cm. Obviously, the pipe has a substantial effect on the beam dynamics in this case. As we expect, the image forces have a focusing effect in the longitudinal direction and a defocusing effect in the radial direction. Also note the coupling between the radial and longitudinal motions. Both planes oscillate synchronously, in phase with the longitudinal envelope equation, as they travel down the beam axis.

V. CONCLUSIONS

It is possible to write a relatively simple set of coupled ordinary differential equations for the rms beam envelopes of an axisymmetric, bunched beam with ellipsoidal symmetry. In the free-space situation we have the differential system given by Eqs. (14), (16), and (17). These equations may be translated to those describing the true beam envelopes of an (approximately) equivalent uniform density bunched beam, which we take to be the uniform density ellipsoid. The equivalent uniform beam has the same second moments, or rms beam envelopes, of the actual beam. This system is represented by Eqs. (24), (16), and (17). When a cylindrical beam pipe is present we represent the image effects in the dynamics equations by the image effects function $A_f(x)$, defined in Eq. (55). This function is plotted in Fig. 5 for four different distributions. In general the function $A_f(x)$ must be computed numerically, say from the integral expressions listed in Table II. In the case of the uniform ellipsoid we have derived an analytic expression involving infinite summations of Bessel functions for $A_f(x)$, which we denote as $A(x)$ for clarity. That expression is given by Eq. (69). The differential system with images is described by Eqs. (71) and (72), where the auxiliary functions are given by Eqs. (16), (17), and (69).

Qualitatively we can make a few generalizations. The beam dynamics are relatively insensitive to the exact form of the distribution in the free-space situation. In this case we can justify the use of an equivalent uniform beam, which we take to be the uniform density ellipsoid, since it has well-defined beam envelopes. That is we can model any bunched beam as a uniform density ellipsoid so long as the uniform beam has the same second spatial moments as the actual beam. On the other hand, when image effects become a factor in the beam dynamics, the distribution's form becomes important. In the presence of images, we no longer have the convenience of an equivalent uniform beam. As mentioned above, the image effects function $A_f(x)$ depends upon the form of the beam's distribution.

The most useful application of these results would seem to be for the case of space-charge-dominated beams, where the stationary distribution is close to a uniform density ellipsoid. In this case the longitudinal image effects from a cylindrical beam pipe would be pronounced due to the large space charge. Since the uniform ellipsoid is ''approximately stationary'' and the dynamics are not sensitive to the beam emittances in the first place, the analysis will be accurate. A complete set of ordinary differential equations has been derived for the uniform density ellipsoid. Once the values of $A(x)$ are tabulated, the differential equations can be easily integrated by standard numerical techniques. Thus, we have a convenient method to simulate the behavior of such beams.

ACKNOWLEDGMENT

This work was supported in part by the U. S. Department of Energy.

APPENDIX A: INTEGRALS

$$\int_0^1 \cos a x I_0(b\sqrt{1-x^2})\,dx$$

$$= \begin{cases} \dfrac{\sinh\sqrt{b^2-a^2}}{\sqrt{b^2-a^2}} & \text{for } a<b \\ \dfrac{\sin\sqrt{a^2-b^2}}{\sqrt{a^2-b^2}} = \operatorname{sinc}\sqrt{a^2-b^2} & \text{for } a>b\,, \end{cases}$$

from Oberhettinger [15], and

$$\int_0^1 x\ \sin(a\sqrt{1-x^2})I_0(bx)dx=\begin{cases}\dfrac{a}{b^2-a^2}\left(\cosh\sqrt{b^2-a^2}-\dfrac{\sinh\sqrt{b^2-a^2}}{\sqrt{b^2-a^2}}\right) & \text{for } a<b\\ \dfrac{a}{a^2-b^2}\left(\dfrac{\sin\sqrt{a^2-b^2}}{\sqrt{a^2-b^2}}-\cos\sqrt{a^2-b^2}\right) & \text{for } a>b\,,\end{cases}$$

from above [16], and

$$\int_0^1 x\ \sin\ axI_0(b\sqrt{1-x^2})dx=\int_0^1 x\ \sin(a\sqrt{1-x^2})I_0(bx)dx=\begin{cases}\dfrac{a}{b^2-a^2}\left(\cosh\sqrt{b^2-a^2}-\dfrac{\sinh\sqrt{b^2-a^2}}{\sqrt{b^2-a^2}}\right) & \text{for } a<b\\ \dfrac{a}{a^2-b^2}\left(\dfrac{\sin\sqrt{a^2-b^2}}{\sqrt{a^2-b^2}}-\cos\sqrt{a^2-b^2}\right) & \text{for } a>b\,.\end{cases}$$

APPENDIX B: FOURIER TRANSFORMS

For a function f, the Fourier transform will be denoted by $\tilde{f}$ and defined by the following:

$$\hat{f}(\omega)=\int_{-\infty}^{+\infty}f(x)e^{-i\omega x}dx.$$

The original function f may be recovered from its transform by the inversion formula

$$f(x)=\frac{1}{2\pi}\int_{-\infty}^{+\infty}\hat{f}(\omega)e^{i\omega x}d\omega.$$

We also introduce the ''sinc'' function which occurs frequently in Fourier analysis. The common definition is

$$\mathrm{sinc}x\equiv\begin{cases}\dfrac{\sin x}{x}, & x\neq 0\\ 1, & x=0\,.\end{cases}$$

Listed below are several functions of the independent variable x and their corresponding Fourier transforms in the variable ω.

$f(x)$	$\hat{f}(\omega)$
1 for $\lvert x\rvert\leqslant a$ 0 for $\lvert x\rvert>a$	$2a\ \mathrm{sinc}a\omega$
$\dfrac{x}{a}$ for $\lvert x\rvert\leqslant a$ 0 for $\lvert x\rvert>a$	$\dfrac{2i}{\omega}\left[\cos a\omega-\mathrm{sinc}a\omega\right]$
$\dfrac{x^2}{a^2}$ for $\lvert x\rvert\leqslant a$ 0 for $\lvert x\rvert>a$	$\dfrac{4\cos a\omega}{a\omega^2}-\dfrac{4\,\mathrm{sinc}a\omega}{a\omega^2}+2a\ \mathrm{sinc}a\omega$
$1-\dfrac{x^2}{a^2}$ for $\lvert x\rvert\leqslant a$ 0 for $\lvert x\rvert>a$	$\dfrac{4}{a\omega^2}\left[\mathrm{sinc}a\omega-\cos a\omega\right]$
$\dfrac{1}{30}-\dfrac{x^2}{8}-\dfrac{x^3}{12}+\dfrac{x^5}{160}$ for $x\in[-2,0]$ $\dfrac{1}{30}-\dfrac{x^2}{8}+\dfrac{x^2}{12}-\dfrac{x^2}{160}$ for $x\in[0,+2]$ 0 for $\lvert x\rvert>2$	$\left(\dfrac{\cos\omega}{\omega^2}-\dfrac{\mathrm{sinc}\omega}{\omega^2}\right)\left(\dfrac{3\cos\omega}{\omega^2}-\dfrac{3\,\mathrm{sinc}\omega}{\omega^2+\mathrm{sinc}\omega}\right)$
$\dfrac{1}{b}\sum_{n=1}^{\infty}\dfrac{1}{J_1(\alpha_n)}e^{-\beta_n\lvert z\rvert}$	$\dfrac{1}{I_0(\omega b)}$ [17]
$\dfrac{1}{2}\dfrac{1}{\sqrt{r^2+z^2}}-\dfrac{1}{b}\sum_{n=1}^{\infty}\dfrac{J_0(\beta_n r)}{\alpha_n J_1^2(\alpha_n)}e^{-\beta_n\lvert z\rvert}$	$K_0(\lvert\omega\rvert b)\dfrac{I_0(\omega r)}{I_0(\omega b)}$ [18]

In the last two transforms $\beta_n=\alpha_n/b$, where α_n is the nth zero of the Bessel function J_0.

[1] O. D. Kellogg, *Foundations of Potential Theory* (Dover, New York, 1953), pp. 192–194.
[2] R. L. Gluckstern, Fermilab Internal Report No. TM-1402, 1986 (unpublished).
[3] T. D. Newton, Can. J. Phys. **44**, 3137 (1966).
[4] D. Neuffer, IEEE Trans. Nucl. Sci. **NS-26**, 3031 (1979).
[5] C. K. Allen, N. Brown, and M. Reiser, Part. Accel. **45**, 149 (1994).
[6] C. K. Allen and M. Reiser, Phys. Rev. E **54**, 2884 (1996).
[7] C. K. Allen and M. Reiser, Part. Accel. **48**, 193 (1995).
[8] F. R. Sacherer, IEEE Trans. Nucl. Sci. **NS-18**, 1105 (1971).
[9] I. M. Kapchinskij and V. V. Vladimirskij, *Proceedings of the International Conference on High-Energy Accelerators and Instrumentation* (CERN, Geneva, 1959), pp. 274–288.
[10] For details of these derivations, see C. K. Allen, Ph.D. disseration, University of Maryland, 1996, Secs, 1.4.4, 3.7.3, and 3.8.3.
[11] Martin Reiser, *Theory and Design of Charged Particle Beams* (Wiley, New York, 1994), Sec. 4.4.
[12] These equations are found using a derivation similar to that of Sacherer in Ref. [5].
[13] The derivation is similar to that done for the Helmholtz equation by I. Stakgold, *Green's Function and Boundary Value Problems* (Wiley, New York, 1979), pp. 459–462.
[14] For a broad description of Fourier transform properties see R. N. Bracewell, *Fourier Transform and its Application*, 2nd ed. (McGraw-Hill, New York, 1978).
[15] F. Oberhettinger, *Table of Fourier Transforms and Fourier Transforms of Distributions* (Springer-Verlag, Berlin, 1990), p. 95.
[16] This integral can be derived from formula 6.738-1 of I. S. Gradshteyn and I. M. Ryzhik, *Table of Integrals, Series and Products*, 5th ed. (Academic, New York, 1994), p. 776. It may also be derived by differentiation the previous integral with respect to a.
[17] This transform is computed directly using the residue theorem, for details of this calculation see Ref. [10], Sec. 3.5.4.
[18] This transform is computed by comparing the two alternate expression for the Green's function; for details of this calculation, see Ref. [10], Sec. 3.5.4.